Tumor Cell Profiling Hot Paper

International Edition: DOI: 10.1002/anie.201608983
German Edition: DOI: 10.1002/ange.201608983

Profiling Functional and Biochemical Phenotypes of Circulating Tumor Cells Using a Two-Dimensional Sorting Device

Mahla Poudineh, Mahmoud Labib, Sharif Ahmed, L. N. Matthew Nguyen, Leyla Kermanshah, Reza M. Mohamadi, Edward H. Sargent, and Shana O. Kelley**

Abstract: *During cancer progression, tumors shed circulating tumor cells (CTCs) into the bloodstream. CTCs that originate from the same primary tumor can have heterogeneous phenotypes and, while some CTCs possess benign properties, others have high metastatic potential. Deconstructing the heterogeneity of CTCs is challenging and new methods are needed that can sort small numbers of cancer cells according to their phenotypic properties. Here we describe a new microfluidic approach that profiles, along two independent phenotypic axes, the behavior of heterogeneous cell subpopulations. Cancer cells are first profiled according to expression of a surface marker using a nanoparticle-enabled approach. Along the second dimension, these subsets are further separated into subpopulations corresponding to migration profiles generated in response to a chemotactic agent. We deploy this new technique and find a strong correlation between the surface expression and migration potential of CTCs present in blood from mice with xenografted tumors. This system provides an important new means to characterize functional diversity in circulating tumor cells.*

Overt metastasis is responsible for as much as 90% of cancer-associated mortality. It is the end result of a multistep process in which circulating tumor cells seed metastatic tumors.[1–4] To metastasize, a CTC must invade, intravasate, extravasate, and grow at a distant site.[5,6] Chemotactic migration mediated by chemokine and growth factors may play an important role in each of these processes.[7–9] Indeed, during intravasation and extravasation, tumor cell migration is influenced by chemotactic factors present in the extracellular matrix.[10] An individual patient's CTCs can be highly heterogeneous, and only those cells that are susceptible to chemotaxis are thought to be involved in the metastatic pathway.[11] CTCs that cannot respond fast enough to chemokines may not participate in the formation of metastatic lesions.

As tumor cells enter into the bloodstream, they can lose their epithelial character and take on a mesenchymal phenotype via the epithelial-to-mesenchymal transition (EMT).[12,13] This phenotypic variation may also contribute to metastatic potential, as the plasticity of cellular properties is believed to be required for intravasation and extravasation. EMT can be tracked by monitoring the surface expression of extracellular or intracellular markers,[14–16] and the analysis of EMT status in CTCs has been shown to be relevant for tracking disease progression. The loss of epithelial characteristics may engender CTCs with greater motility that supports the invasion of secondary sites.[5,7]

Microfluidic isolation of rare cells opens new venues to study CTCs;[16–24] however, existing techniques simply capture and enumerate CTCs and do not analyze phenotypically the heterogeneous cancer cell subpopulations encountered in clinical specimens. Given the functional diversity of CTC subpopulations,[25,26] enumeration of CTCs alone is inadequate to understand their behavior. While microfluidic devices have been employed to study the migration of cancer cells toward a chemoattractant, systems that are applicable to blood-borne CTCs are lacking. Many different aspects of cancer cell migration and invasion have been studied using microfluidic devices,[27–33] but previous studies were confined to the study of cultured cancer cells rather than true CTCs obtained from blood samples.

Our profiling approach relies on fluidic capture and phenotypic sorting of heterogeneous subpopulations of cancer cells. In the first sorting dimension, cells are sorted into one of four zones based on levels of surface marker expression (Figure 1 and Figure S1). The epithelial cell adhesion molecule (EpCAM) was chosen as an initial profiling target since it is a well-characterized marker present on the surface of many different types of cancer cells and has levels that are known to vary during cancer progression.[1,34] Other proteins known to be important markers of EMT could also be targeted using this same strategy.[26,35] The sorting is achieved according to levels of bound aptamer-functionalized magnetic nanoparticles (aptamer-MNP, Figure 1) that report on EpCAM expression.[36] The zones that are patterned within our microfluidic device feature microfabricated X-structures to adjust the required drag force for cell capture. Previous studies of this approach have demonstrated high cell capture efficiencies of cultured cells and CTCs using this

[*] M. Poudineh, Prof. E. H. Sargent
Department of Electrical and Computer Engineering
University of Toronto, Toronto, ON (Canada)
E-mail: ted.sargent@utoronto.ca
Dr. M. Labib, Dr. S. Ahmed, L. N. M. Nguyen, Dr. R. M. Mohamadi, Prof. S. O. Kelley
Leslie Dan Faculty of Pharmacy
University of Toronto, Toronto, ON (Canada)
E-mail: shana.kelley@utoronto.ca
L. Kermanshah, Prof. S. O. Kelley
Institute of Biomaterials and Biomedical Engineering
University of Toronto, Toronto, ON (Canada)
Prof. S. O. Kelley
Department of Biochemistry
University of Toronto, Toronto, ON (Canada)
Supporting information and the ORCID identification number(s) for the author(s) of this article can be found under http://dx.doi.org/10.1002/anie.201608983.

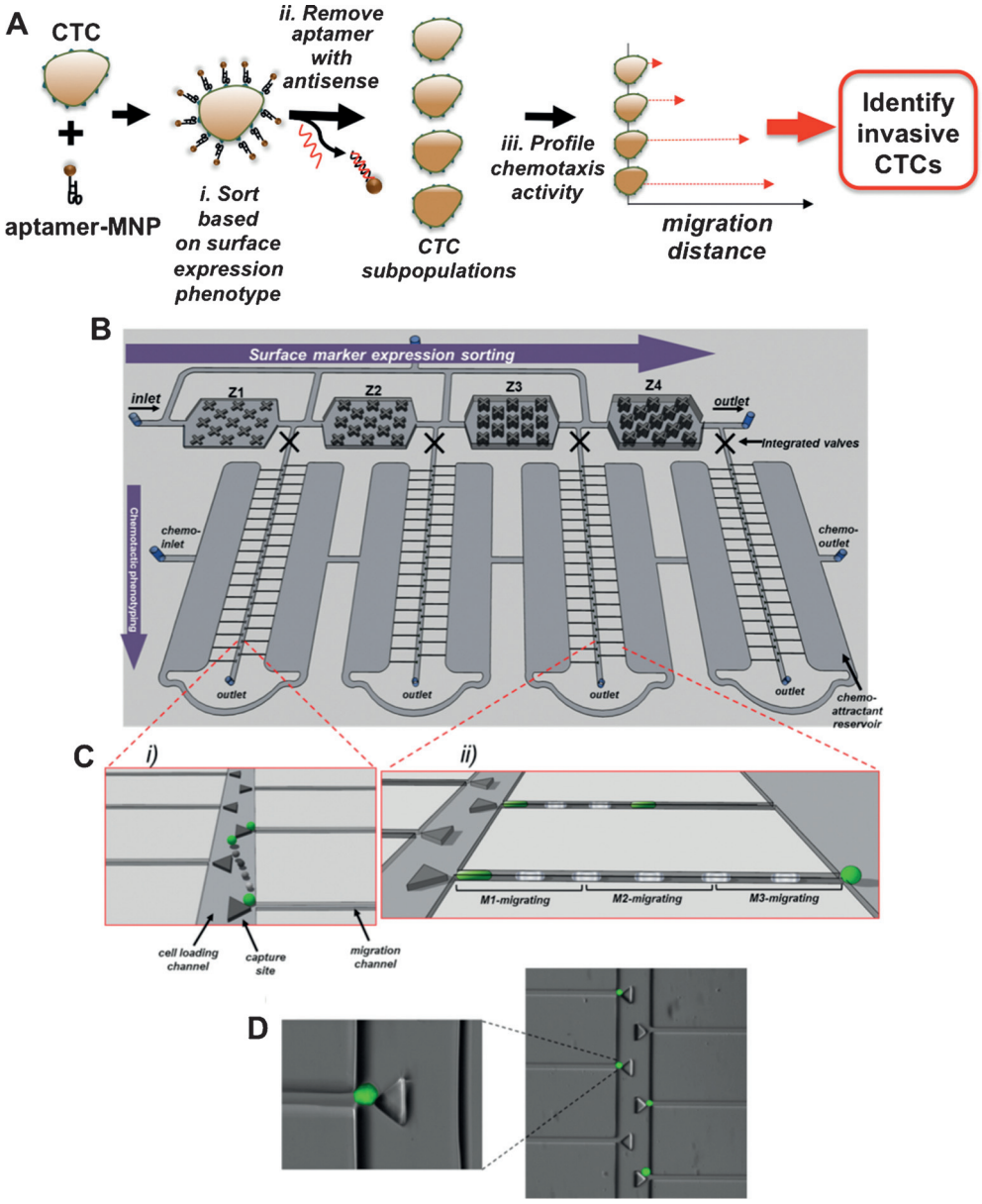

Figure 1. Profiling functional and biochemical phenotypes of CTCs. A) Overview of two-dimensional characterization approach. B) Cells are first sorted according to the levels of a surface marker, for example, EpCAM. High- and low-EpCAM cells are captured in Z1 and Z4, respectively. After EpCAM sorting, cell subpopulations extracted from each zone are subjected to chemotactic phenotype sorting. C) Magnified images of the chemotaxis chip. i) Microfabricated traps located in the cell-loading channel are used as the capture sites. When a cell is captured at one trap site, the captured cell blocks the flow through one side of the channel, and remaining cells are subsequently captured at the downstream capture sites. ii) The cell loading channel is connected to the chemoreservoir through the migration channels. Cells migrate from the cell-loading channel toward the chemoattractant reservoir. The migration channel is divided into three regions to study the migration of different cell subpopulations more effectively. D) Image of captured cells in the cell loading channel.

technique.[14,15] Changing the cross-sectional area of the microfluidic channel alters the linear velocity (and thus the drag force acting on the CTCs), enabling the capture of distinct subpopulations of cancer cells exhibiting different levels of surface marker expression. The first zone has the highest linear velocity (produced by a small cross-sectional area) and retains cells having high levels of the surface marker. The succeeding three zones exhibit reduced linear velocities, each decreasing the velocity by twofold. Consequently, the lowest linear velocity at the fourth zone facilitates the accumulation of low-expression cells. After binning the subpopulations into four successive zones, we released the cells using the antisense DNA strand complementary to the capture aptamer.[36] As previously described,[14,15] this subpopulation-sorting chip yields results similar to those obtained using flow cytometry, and produces discrete profiles for high-EpCAM cells (e.g. LNCaP cells) versus low-EpCAM cells (e.g. PC3 cells, Figure S2).

After the subpopulations are separated according to levels of surface expression, a second dimension of CTC sorting is applied that characterizes a functional phenotype for cancer cells that is believed to be linked directly with metastatic potential: cell migration via chemotaxis. The chemotactic sorting process in our device relies on the migration of extracted cell subpopulations toward a specific chemoattractant. Four chemotaxis modules are connected to the four zones of the surface marker expression sorting device that allow us to study the migration behavior of cell subpopulations (Figure 1 B). Each chemotaxis chip contains one cell-loading channel that is connected to two chemoattractant reservoirs through migration channels.

Microfabricated traps inside the cell-loading channel are used as the capture sites (Figure 1 C, left and Figure 1 D). Prior to the loading of cells, the desired chemoattractant is loaded into chemoreservoirs; the reservoirs are separated from the cell-loading and migration channels via valves that are initially closed (Figure S1). These valves are used to prevent chemoattractant diffusion into the migration and cell-loading channels during cell capture. After chemoattractant

loading, cells that are released flow toward the cell-loading channel and are captured at the ensuing trap sites.

Captured cells migrate toward the chemical gradient generated in the migration channel. When the valves are open, the concentration of chemoattractant increases linearly along the migration channel, as confirmed by simulations (Figure S3B and Figure S4). After 3 hours, a linear gradient of chemoattractant is generated along the migration channels (Figure S3C,D).

To study single-cell migration behavior more quantitatively, we divided each migration channel into three regions (Figure 1 C, right). This channel division makes it possible to distinguish between highly mobile cells and cells with less pronounced chemotaxis phenotypes. After an incubation period where cells are permitted to migrate, they are categorized as either non-migrating, M1 (minimal migration), M2 (intermediate migration), M3 (high migration), or migrated.

First, we explored the performance of the chemotaxis chip to ensure that it would report on the migratory properties of CTCs. Two model prostate cancer cell lines and two model breast cancer cell lines[37] were chosen to challenge the effectiveness of the chemotaxis chip. The desired chemoattractant was prepared in serum-free media and loaded into chemoreservoirs before cell injection. In order to verify the effect of chemoattractant on cell migration, we performed control experiments using a serum-free medium instead of the chemoattractant.

Migration results for PC3 (a metastatic prostate cancer cell line) and LNCaP (a less aggressive prostate adenocarcinoma cell line) cells are shown in Figure 2 A and B, respectively. We selected CXCL16 as a chemoattractant to

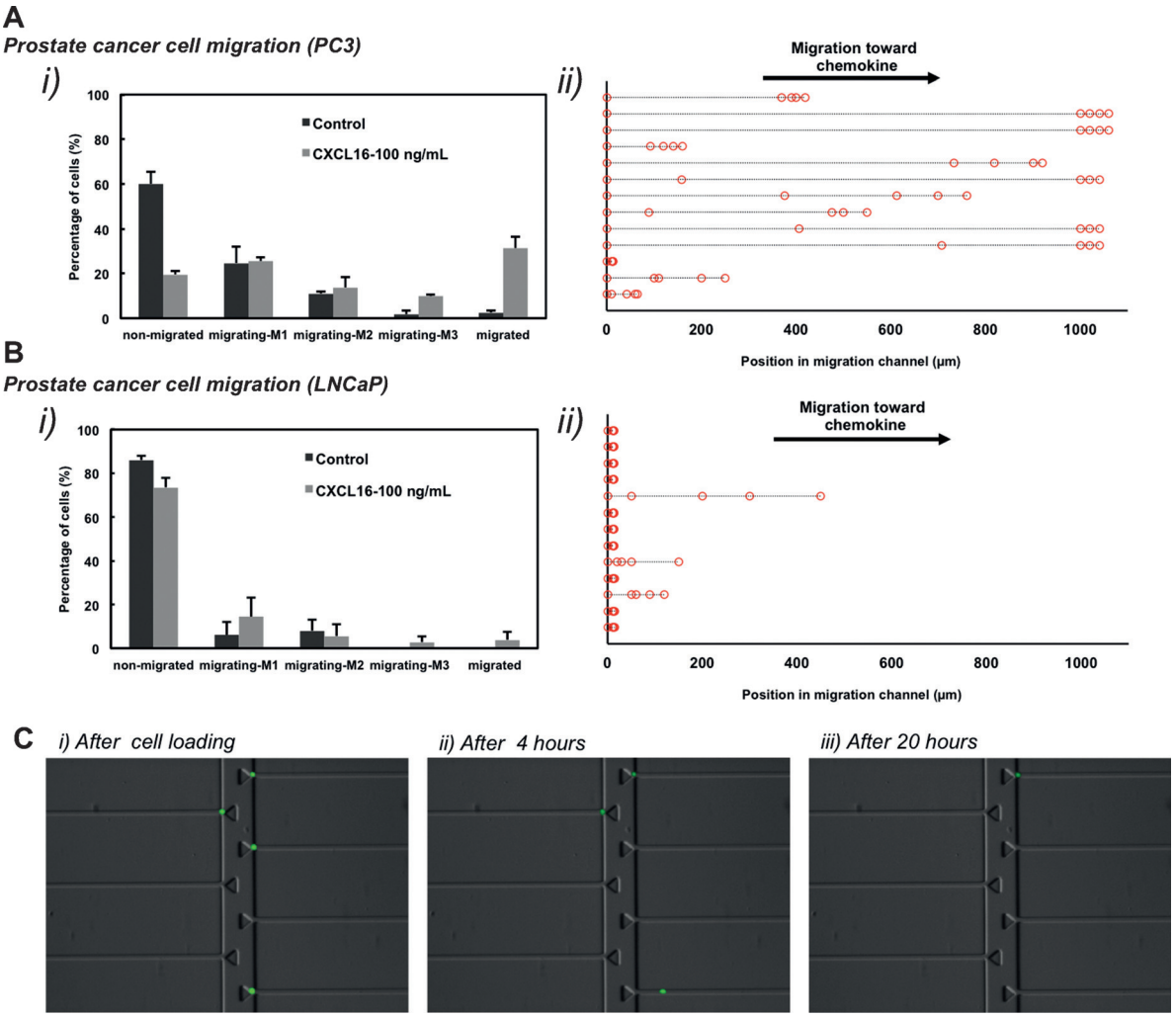

Figure 2. Chemotactic phenotype sorting of model prostate cancer cell lines. A) Chemotactic migration of aggressive (PC3) prostate cancer cell line in response to 100 ng mL^{-1} of CXCL16 as a chemoattractant. i) Results show that CXCL16 induces migration in PC3 cells. ii) PC3 migration was monitored at different time points: 0 h, 5 h, 10 h, 15 h, and 20 h after cell loading. The position of 13 cells was measured at each time point. Each red circle denotes the cell position at one time point. Results show that more than 35% of PC3 cells migrated in the first 5 hours of incubation. B) Chemotactic migration of non-aggressive (LNCaP) prostate cancer cell lines in response to CXCL16 as the chemoattractant. i) Results demonstrate that LNCaP migration in response to the CXCL16 is negligible. ii) LNCaP migration was observed at different time points. Less than 25% of cells migrated toward chemoattractant. C) Images of the single-cell migration assay. PC3 cells were loaded in the cell-loading channel and 100 ng mL^{-1} of CXCL16 was used as the chemoattractant. The left image illustrates the single-cell distribution after cell loading. The middle and right images show the cell distribution after 4 and 20 hours incubation, respectively.

study prostate cancer cell migration behavior, as it has been shown that CXCL16 induces prostate cancer cell migration and may play an important role in prostate cancer progression.[38] In experiments with PC3 cells, more than 40% of PC3 cells either migrated completely toward the chemoreservoirs or were found in the last one-third of migration channel (M3). The migration of LNCaP cells, however, was much less pronounced (Figure 2B). We also monitored CXCL16-stimulated migration for both PC3 and LNCaP cells at different time points (0 h, 5 h, 10 h, 15 h, and 20 h after cell loading). Most of the PC3 cells begin to migrate within 5 hours, and roughly one-third are completely migrated within this time window. The migration profiles as a function of time for the LNCaP cells support the conclusion that these cells are not able to respond to a chemoattractant efficiently. Figure 2C shows time-lapse images corresponding to the migration of PC3 cells.

The investigation of chemotactic migration of both prostate (Figure 2) and breast cancer (Figure S5) cells reveals that mesenchymal character increases the motility of cells. The two cell lines with greater mesenchymal character (PC3 and MDA-MB-231) showed higher mobility than the epithelial cell lines (LNCaP and MCF-7). These results demonstrate that the proposed chemotaxis chip profiles cells according to their response to a chemical stimulator, and also that it enables evaluation of single-cell migration behavior. Cells having different levels of invasiveness exhibited distinct migration profiles.

We proceeded to evaluate whether an integrated sorting system could monitor 2D phenotypic properties of cells present in unprocessed whole blood. Whole blood samples were spiked with PC3 cells, and following EpCAM-based sorting of the cells into four different subpopulations, CXCL16 was used to stimulate chemotactic migration of extracted cell subpopulations. The results (Figure 3 and Figure S6) confirm that cancer cell subpopulations with different levels of EpCAM expression exhibit different migration profiles. Compared to cell subpopulations extracted from the high-EpCAM zone, low-EpCAM cells demonstrated increased migration tendency upon stimulation with chemoattractant.

The integrated system was challenged using blood from mice bearing xenografted tumors to evaluate the utility of this system for the analysis of CTCs. Three prostate cancer cell lines (LNCaP, PC3, and PC3M) were implanted orthotopically into immunodeficient mice. PC3 and PC3M cells are known to have high metastatic potential while LNCaP cells possess more benign properties. Mice were sacrificed 4 weeks after tumor cell injection and 700 μL of their blood was collected for analysis using the two-dimensional phenotypic profiling approach.

The profiles of CTCs (Figure 4A) extracted from three xenograft models are shown in Figure 4 and Figure S7. In all of the xenografted animals, significant numbers of CTCs were detected. The CTCs from animals xenografted with LNCaP tumors exhibited downregulated EpCAM expression (Figure 4B) relative to the ungrafted cell line (Figure S2), but very few cells showed significant levels of chemotaxis. For the animals with PC3-derived tumors, the majority of CTCs in the later zones of the device exhibited high levels of migratory behavior. In addition, the PC3M-derived tumors produced CTCs that displayed efficient chemotaxis, especially for cells that were sorted into the low-EpCAM zones of the device.

In order to evaluate the levels of metastasis produced by the xenografted tumors, we extracted the lungs and lymph nodes from two mice in each group and sent them for

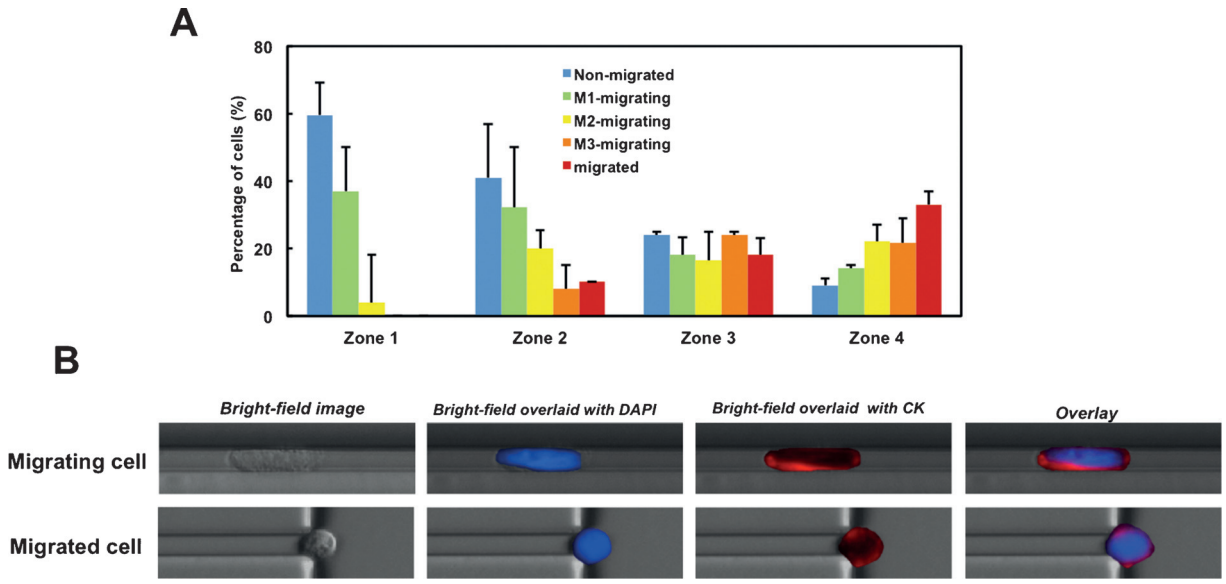

Figure 3. Validation of 2D sorting approach. A) 2D phenotypic sorting chip was applied to PC3 cells in whole blood samples. The first sorting step was performed based on EpCAM expression using an EpCAM-specific aptamer tagged with magnetic nanoparticles. After release of the cells using the corresponding antisense DNA, AS-EpCAM1, cell subpopulations extracted from each zone were subjected to chemotactic phenotype sorting. CXCL16 (100 ng mL^{-1}) was used as the chemoattractant. In total, a recovery efficiency of 79 ± 4% was achieved after cell capture in the second dimensional profiling. B) Immunofluorescence images of a migrating cell (inside the channel) and a migrated cell (ejected into the chemoreservoir).

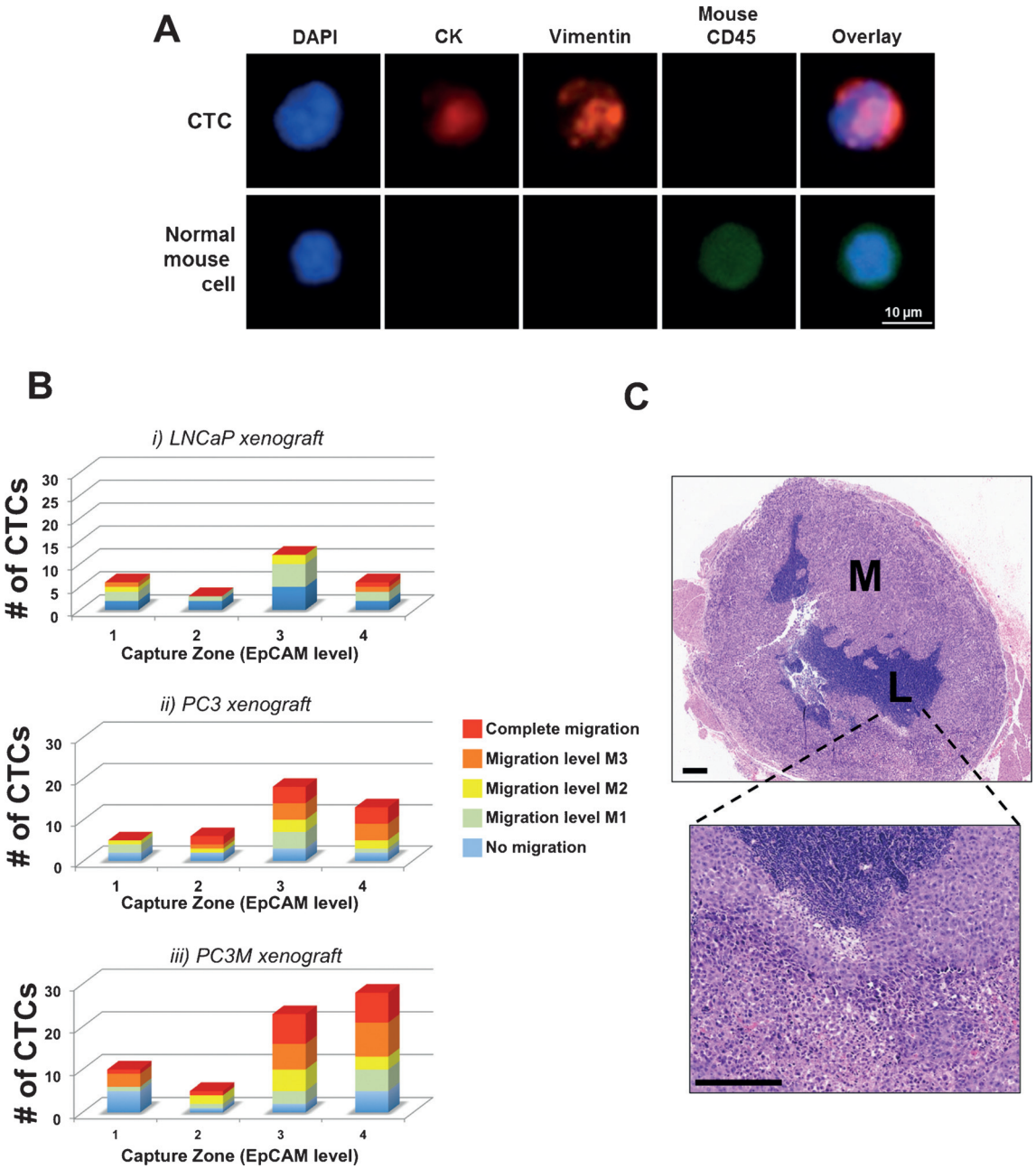

Figure 4. 2D phenotypic profiling of CTCs in cancer xenograft models. First, CTCs were sorted based on their EpCAM expression. Subsequent to the releasing of CTCs using the corresponding antisense, CTC subpopulations extracted from each zone were subjected to the chemotactic phenotype sorting. CXCL16 (100 ng mL^{-1}) was used as the chemoattractant. A) Representative images of a captured CTC and a normal mouse cell. Nuclei are stained with DAPI (blue), CTCs are stained for CK (red) and Vimentin (orange), and mouse cells for mouse CD45 (green). B) 2D phenotypic profiles of CTCs extracted from mice in cancer xenograft models. Total numbers of captured CTCs are: 27, 42, and 66 in LNCaP, PC3, and PC3M xenografts, respectively. See Figure S7 for additional data collected with animals. C) Histopathology image of lymph node section of a mouse in PC3M xenograft confirming the presence of micro-metastases. The metastases (M) almost completely affected normal lymph node architecture and only small amounts of lymphoid tissue (L) remained. Scale bars are 250 µm.

histopathology. Micro-metastases were found in the lung and lymph nodes of animals that also displayed high levels of migratory behavior (Figure 4C). 86 micro-metastases were found in the organs of mice with PC3M tumors and 2 micro-metastases were found in mice with PC3 tumors. However, the scans of lungs and lymph nodes of mice with LNCaP tumors did not yield any micro-metastases. This trend indicates that the migratory properties of CTCs—which can be visualized straightforwardly with our device—may indeed correlate with their metastatic potential.

The technique described here can be used to isolate phenotypically distinct cell subpopulations defined using two phenotypes—a biochemical phenotype reporting on EMT status, and a functional phenotype reporting on migratory

potential. The two phenotypes appear to be correlated: both in cultured cells and CTCs collected in animal xenografts, the loss of epithelial character correlates with efficient chemotaxis. Indeed, in the most invasive xenograft studied (PC3M), the CTCs showed low EpCAM levels, and almost 50% of CTCs exhibited significant migratory activity. The presence of micro-metastases also confirmed high metastatic potential of migratory CTCs.

The approach described herein reveals phenotypic profiles of low levels of CTCs in unprocessed blood samples. The high levels of sensitivity obtained and compatibility with whole blood makes this technique a powerful tool for the analysis of rare circulating tumor cells. 2D phenotypic profiling is an effective strategy for CTC profiling that allows the heterogeneous phenotypes of CTCs to be monitored.

Acknowledgements

We acknowledge generous support from the Canadian Institutes of Health Research (Emerging Team grant, POP Grant), the Ontario Research Fund (ORF Research Excellence grant), the Canadian Cancer Society Research Institute (Innovation grant), and the Connaught Foundation.

Conflict of interest

The authors declare no conflict of interest.

Keywords: aptamers · cancer · chemotaxis · microfluidic devices · surface marker expression

How to cite: *Angew. Chem. Int. Ed.* **2017**, *56*, 163 – 168
Angew. Chem. **2017**, *129*, 169 – 174

[1] K. Pantel, C. Alix-Panabières, S. Riethdorf, *Nat. Rev. Clin. Oncol.* **2009**, *6*, 339 – 351.
[2] K. Pantel, R. H. Brakenhoff, *Nat. Rev. Cancer* **2004**, *4*, 448 – 456.
[3] C. L. Chaffer, R. A. Weinberg, *Science* **2011**, *331*, 1559 – 1564.
[4] V. Plaks, C. D. Koopman, Z. Werb, *Science* **2013**, *341*, 1186 – 1188.
[5] E. T. Roussos, J. S. Condeelis, A. Patsialou, *Nat. Rev. Cancer* **2011**, *11*, 573 – 587.
[6] D. Hanahan, R. A. Weinberg, *Cell* **2011**, *144*, 646 – 674.
[7] F. Balkwill, *Nat. Rev. Cancer* **2004**, *4*, 540 – 550.
[8] M. T. Chow, A. D. Luster, *Cancer Immunol. Res.* **2014**, *2*, 1125 – 1131.
[9] T. Kakinuma, S. T. Hwang, *J. Leukocyte Biol.* **2006**, *79*, 639 – 651.
[10] W. G. Stetler-Stevenson, S. Aznavoorian, L. A. Liotta, *Annu. Rev. Cell Biol.* **1993**, *9*, 541 – 573.
[11] P. S. Steeg, *Nat. Med.* **2006**, *12*, 895 – 904.
[12] I. Lokody, *Nat. Rev. Cancer* **2014**, *14*, 152.
[13] J. M. Lang, B. P. Casavant, D. J. Beebe, *Sci. Transl. Med.* **2012**, *4*, 1 – 5.
[14] J. D. Besant, R. M. Mohamadi, P. M. Aldridge, Y. Li, E. H. Sargent, S. O. Kelley, *Nanoscale* **2015**, *7*, 6278 – 6285.
[15] R. M. Mohamadi, J. D. Besant, A. Mepham, B. Green, L. Mahmoudian, T. Gibbs, I. Ivanov, A. Malvea, J. Stojcic, A. L. Allan et al., *Angew. Chem. Int. Ed.* **2015**, *54*, 139 – 143; *Angew. Chem.* **2015**, *127*, 141 – 145.
[16] E. Ozkumur, A. M. Shah, J. C. Ciciliano, B. L. Emmink, D. T. Miyamoto, E. Brachtel, M. Yu, P. Chen, B. Morgan, J. Trautwein et al., *Sci. Transl. Med.* **2013**, *5*, 179ra47.
[17] A. Adams, P. I. Okagbare, J. Feng, M. L. Hupert, D. Patterson, J. Go, *J. Am. Chem. Soc.* **2008**, *130*, 8633 – 8641.
[18] S. L. Stott, C. Hsu, D. I. Tsukrov, M. Yu, D. T. Miyamoto, B. A. Waltman, S. M. Rothenberg, A. M. Shah, M. E. Smas, G. K. Korir et al., *Proc. Natl. Acad. Sci. USA* **2010**, *107*, 18392 – 18397.
[19] K. Hoshino, Y.-Y. Huang, N. Lane, M. Huebschman, J. W. Uhr, E. P. Frenkel, X. Zhang, *Lab Chip* **2011**, *11*, 3449 – 3457.
[20] S. Nagrath, L. V Sequist, S. Maheswaran, D. W. Bell, D. Irimia, L. Ulkus, M. R. Smith, E. L. Kwak, S. Digumarthy, A. Muzikansky et al., *Nature* **2007**, *450*, 1235 – 1239.
[21] A. H. J. Yang, T. H. Soh, *Anal. Chem.* **2012**, *84*, 10756 – 10762.
[22] W. Sheng, T. Chen, W. Tan, Z. Hugh, *ACS Nano* **2013**, *7*, 7067 – 7076.
[23] J. Che, V. Yu, M Dhar, C. Renier, M. Matsumoto, K. Heirich, E. B. Garon, J. Goldman, J. Rao, G. W. Sledge et al., *Oncotarget* **2016**, *7*, 12748 – 12760.
[24] B. Green, T. Saberi Safaei, A. Mepham, M. Labib, R. M. Mohamadi, S. O. Kelley, *Angew. Chem. Int. Ed.* **2016**, *55*, 1252 – 1265; *Angew. Chem.* **2016**, *128*, 1270 – 1284.
[25] X. Yao et al., *Integr. Biol.* **2014**, *6*, 388 – 398.
[26] R. Königsberg, E. Obermayr, G. Bises, G. Pfeiler, M. Gneist, F. Wrba, M. de Santis, R. Zeillinger, M. Hudec, C. Dittrich, *Acta Oncol.* **2011**, *50*, 700 – 710.
[27] S. P. Desai, S. N. Bhatia, M. Toner, D. Irimia, *J. Biophys.* **2013**, *104*, 2077 – 2088.
[28] Y. G. Ko, C. C. Co, C. C. Ho, *Soft Matter* **2013**, *9*, 2467 – 2474.
[29] S. Chung, R. Sudo, P. J. Mack, C. R. Wan, V. Vickerman, R. D. Kamm, *Lab Chip* **2009**, *9*, 269 – 275.
[30] Y. Zhang, W. Zhang, L. Qin, *Angew. Chem. Int. Ed.* **2014**, *53*, 2344 – 2348; *Angew. Chem.* **2014**, *126*, 2376 – 2380.
[31] Y.-C. Chen, S. G. Allen, P. N. Ingram, R. Buckanovich, S. D. Merajver, E. Yoon, *Sci. Rep.* **2015**, *5*, 9980.
[32] I. Y. Wong, S. Javaid, E. A. Wong, S. Perk, D. A. Haber, M. Toner, D. Irimia, *Nat. Mater.* **2014**, *13*, 1063 – 1071.
[33] S. H. Au et al., *Proc. Natl. Acad. Sci. USA* **2016**, *113*, 4947 – 4952.
[34] M. Yu, A. Bardia, B. S. Wittner, S. L. Stott, M. E. Smas, D. T. Ting, S. J. Isakoff, J. C. Ciciliano, M. N. Wells, A. M. Shah et al., *Science* **2013**, *339*, 580 – 584.
[35] T. M. Gorges, I. Tinhofer, M. Drosch, L. Rose, T. M. Zollner, T. Krahn, O. von Ahsen, *BMC Cancer* **2012**, *12*, 178.
[36] M. Labib, B. Green, R. M. Mohamadi, A. Mepham, S. U. Ahmed, L. Mahmoudian, I.-H. Chang, E. H. Sargent, S. O. Kelley, *J. Am. Chem. Soc.* **2016**, *138*, 2476 – 2479.
[37] S.-J. Wang, W. Saadi, F. Lin, C. Minh-Canh Nguyen, N. Li Jeon, *Exp. Cell Res.* **2004**, *300*, 180 – 189.
[38] R. Singh, N. Kapur, H. Mir, N. Singh, J. W. Lillard Jr, S. Singh, *Oncotarget* **2016**, *7*, 7343 – 7353.

Manuscript received: September 13, 2016
Revised: November 1, 2016
Final Article published: November 29, 2016

